Malaysian Journal of Chemistry, 2021, Vol. 23(4), 115-123
(Special Issue: 3rd Virtual Symposium on Multidisciplinary Science 2021 (V-SMS2021))

Molecular Dynamics Simulation of Collagen Binding to an Amyloid-Beta Monomer and its Effect on the Peptide Structure

Norzalina Zakaria[2,3], Nur Hana Faujan[1,2*], Muhammad Alif Mohammad Latif[1,2], Siti Nor Ani Azaman[1], Intan Diana Mat Azmi[1], Nadiatul Hafiza Hassan[1] and Muhammad Fitri bin Azhar[3]

[1]Center of Foundation Studies for Agricultural Science, Universiti Putra Malaysia, 43400 Serdang UPM, Selangor, Malaysia
[2]Integrated Chemical Biophysics Research, Faculty of Science, Universiti Putra Malaysia, Serdang, Selangor, Malaysia
[3]Department of Chemistry, Faculty of Science, Universiti Putra Malaysia, 43400 UPM, Serdang, Selangor, Malaysia
*Corresponding author (e-mail: nurhana@upm.edu.my)

Alzheimer's disease (AD) is a progressive neurodegenerative disease associated with the accumulation of amyloid beta (Aβ) peptides in the central nervous system (CNS). The extracellular matrix (ECM) proteins play an important role in the AD process. Fibrillar type III collagen is one of the major constituents of the ECM, providing the tissue with tensile strength and influencing cell attachment and migration. However, its structural properties and the binding mechanism of the $A\beta_{42}$ monomer with type III collagen at the molecular level are largely unknown. In this study, the binding interactions of type III collagen with the $A\beta_{42}$ monomer and the conformational dynamics of the $A\beta_{42}$ monomer were investigated through molecular docking and molecular dynamics (MD) simulations. Docking results showed that type III collagen formed hydrogen bonds and hydrophobic contacts with the N-terminal, hydrophobic (CHC and SHR) and C-terminal regions of the $A\beta_{42}$ monomer. Whereas MD results revealed that type III collagen reduced the helical content and promoted an aggregation-prone β-sheet conformation in the $A\beta_{42}$ peptide structure. This finding suggests that type III collagen, and possibly other collagens, may play a role in regulating amyloid fibril formation. The results indicate that the localization of type III collagen may be an important initial event in amyloid plaque formation. Thus, our findings provide a preliminary understanding of the interaction of the Aβ peptide with type III collagen in Alzheimer's disease.

Key words: Type III collagen; Aβ peptide; Alzheimer's disease; Molecular docking, Molecular dynamics

Received: June 2021; Accepted: October 2021

Alzheimer's disease (AD) is a progressive, neurodegenerative disorder associated with memory loss and cognitive decline [1]. The "amyloid cascade hypothesis" suggested that aggregation and deposition of the Aβ peptide in neurons was the key to AD [2]. The Aβ peptide is formed from sequential cleavage of AβPP (a transmembrane precursor protein) by β- and γ-secretases via the amyloidogenic pathway, producing two dominant alloforms, $A\beta_{40}$ and $A\beta_{42}$ that consist of 40 and 42 amino acids, respectively. While initially unstructured when released extracellularly, Aβ undergoes misfolding, which results in the appearance of β-sheet structures. The appearance of β-sheet structures ultimately leads to the self-association of peptide monomers to form toxic species [3].

Cumulative evidence suggests that the extracellular matrix (ECM) in the brain plays an important role in the etiology of AD [4]. The ECM is a meshwork of proteins and carbohydrates that supports many biological structures and processes, from tissue development and elasticity to preserving the structures of entire organs. In the central nervous system (CNS), fibrous proteins (collagen, elastin) and adhesive glycoproteins (laminin, fibronectin) are widely found to maintain the mechanical strength and elasticity of the ECM [5,6]. The biomechanical properties of the neuronal ECM are essential to neurogenesis, neuronal migration, neurite outgrowth, and synaptic plasticity [6,7]. However, when ECM functions aberrantly in brains, it may induce neurodevelopmental disorders, psychiatric dysregulation, and neurodegenerative diseases [8,9].

Collagens are broadly distributed in ECM as fibrillar proteins and structurally host resident cells. There are 28 different types of collagen that assemble into a variety of supramolecular structures. ECM collagens are reported be linked to amyloidosis and neuroprotection in the AD process. For example,

†Paper presented at the 3rd Virtual Symposium on Multidisciplinary Science 2021 (V-SMS2021)

collagen VI blocked neuron-Aβ_{42} oligomer interactions in cultured neurons and prevented neurotoxicity [10]. Other research reported that soluble collagen XXV inhibited fibrillization of Aβ in vitro, especially in the elongation phase. However, it was also reported that the incubation of soluble collagen XXV with Aβ fibrils in vitro lead to larger aggregates [11]. The current research cannot clearly explain the role of collagen in AD pathogenesis. Therefore, further investigation is required to demonstrate the multiple effects of different types of collagen in AD pathogenesis.

In the present study, molecular docking and molecular dynamics (MD) simulations were employed to study the binding interactions of ECM type III collagen with the Aβ_{42} monomer and the conformational dynamics of the Aβ_{42} peptide in the presence of type III collagen. The Docking result highlighted that type III collagen forms hydrogen bonds and hydrophobic contacts with with N-terminal, hydrophobic (central hydrophobic core (CHC) and second hydrophobic region (SHR)) and C-terminal regions of Aβ_{42} monomer. Whereas MD results highlighted that type III collagen reduced the helical content and promoted aggregation-prone β-sheet conformation in the Aβ_{42} peptide structure.

MATERIALS AND METHODS

Molecular Docking

Molecular docking was performed to examine the complex interactions of type III collagen with the Aβ_{42} peptide. To this aim, three dimensional (3D) structures of each counterpart (type III collagen, PDB ID: 1BKV [12] and Aβ_{42} peptide, PDB ID: 1Z0Q [13]) (Figure 1) were first obtained from the Protein Data Bank and then submitted to HDOCK server, a highly integrated suite for robust and fast protein–protein docking [14]. The first mode 3D configuration of PDB ID: 1Z0Q was assigned for the Aβ_{42} peptide to be docked against the type III collagen (hereafter referred to as the 1BKV collagen) with a 100 number conformational search. The server automatically predicts their interaction using a hybrid algorithm of template-based modelling and *ab-initio* template-free docking. The quantitative values of the docking results **were** evaluated by docking scores**.** The best conformation of each ligand against the Aβ_{42} peptide in 100 numbers of conformational searching was identified by its lowest energy value. The top 100 predicted complex structures were downloaded and the top 10 models were visualized using Biovia Discovery Studio Visualizer 2019 [15].

Molecular Dynamics Simulations

MD simulations were performed using the GROMACS 5.1.4 package [16] with the GROMOS96 43A1 force field [17], which has been widely used for the conformational change analysis of Aβ [18–24]. The Aβ_{42} and the docked complex of Aβ_{42}-1BKV obtained from the HDOCK server were selected for MD simulations and the two systems were named Aβ_{42}-APO and Aβ_{42}-1BKV complex, respectively. An auxiliary program of GROMACS, "gmx pdb2gmx" was used to generate the topology of the Aβ_{42} peptide and 1BKV collagen. Each system was placed in a cubic box and a minimum distance of 1.0 nm was kept from the Aβ_{42} peptide and Aβ_{42}-1BKV complex to the edge of the box. Both systems were solvated with water molecules using a simple point charge (SPC) water model and neutralized with counterions [25]. The long-range electrostatic interactions were evaluated using the particle mesh Ewald (PME) method and the short-range van der Waals interactions cut off was kept at 1.0 nm [26]. The bond lengths were

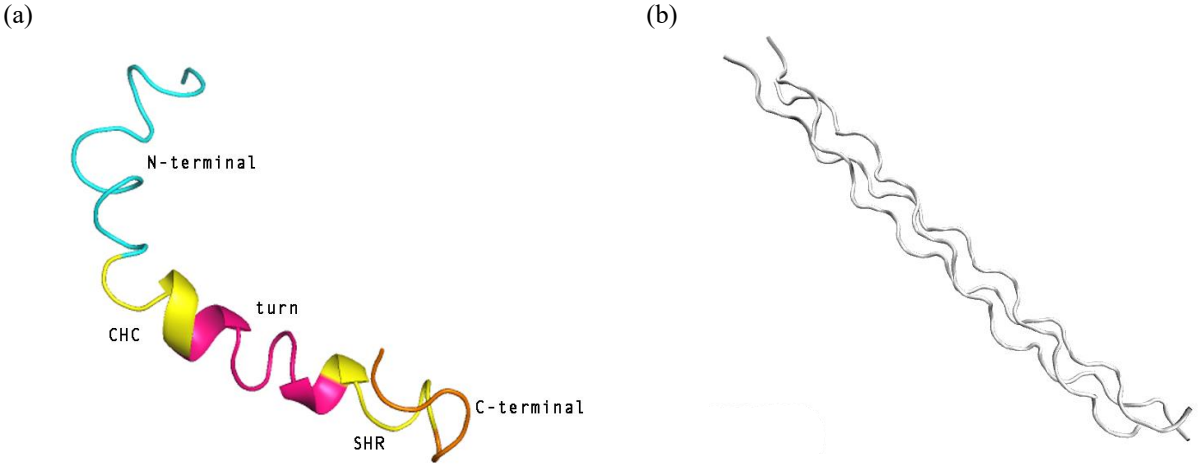

Figure 1. A cartoon representation of Aβ_{42} peptide (PDB ID: 1Z0Q) is shown in (a). The N-terminal (residue 1-15), turn (residue 21-28) and C-terminal (residue 36-42) are shown in blue, pink and orange, respectively. Whereas, the hydrophobic regions, CHC (residue 16-20) and SHR (residue 29-35) are shown in yellow. A cartoon representation of type III collagen (PDB ID: 1BKV) is shown in (b).

constrained using the LINCS algorithm with an integration time step of 2 fs followed by energy minimization using a steepest descent integrator [27]. The systems were equilibrated for 300 ps under NVT and the temperature was kept at 310 K. Then, the systems were further equilibrated for 300 ps under an NPT ensemble at 1 atm. After the equilibration steps, 50 ns explicit MD simulations were performed for both systems under an NPT ensemble with 2 fs leapfrog integration [28]. Temperature (310 K, which is the average human body temperature) and pressure (1 atm) were controlled by the V-rescale thermostat [29] and Parrinello-Rahman barostat [30] respectively.

The auxiliary programs of GROMACS ("gmx rms", "gmx gyrate", "gmx sasa" and "gmx hbond") were used along with Biovia Discovery Studio Visualizer 2019 to visualize and analyze MD trajectories. The Dictionary of Secondary Structure of Proteins (DSSP) program [31] was utilized to analyze the secondary structures of the Aβ42-APO and Aβ42-1BKV complexes. The structural analysis of the conformational ensemble was performed by evaluating root-mean-square deviation (RMSD) and radius-of-gyration (Rg) using "gmx rms" and "gmx gyrate", respectively. The solvent-accessible surface area (SASA) per residue was computed using "gmx sasa" which evaluated the area of the residue exposed to solvent. The hydrogen bonds were evaluated using "gmx hbond".

RESULT AND DISCUSSION

The molecular docking studies revealed that 1BKV collagen binds preferably to the N-terminal, hydrophobic segments (CHC and SHR) and C-terminal regions of the initial structure of Aβ42 with a HDOCK score of -205.30 kcalmol^{-1}. The CHC and C-terminal region is known to play a critical role in Aβ42 aggregation [3]. 1BKV collagen forms two hydrogen bonds with Arg5 and Asp23 of Aβ42 with distances of 3.14 nm and 1.76 nm, respectively. The 3D binding interactions (Figure 2) obtained from Biovia Discovery Studio Visualizer [15] displayed that 1BKV collagen formed hydrophobic contacts with residues of N-terminal (Phe4, Val12), CHC (Phe19, Phe20), SHR (Ile31) and C-terminal (Val40, Ile41, Ala42) regions of the Aβ42 monomer (Table 1). The docking results highlighted the role of hydrogen bonding interactions and hydrophobic contacts for the effective binding of 1BKV collagen with the Aβ42 peptide.

Table 1. Molecular docking analysis of Aβ42 with 1BKV collagen.

Ligand	HDOCK score (kcal mol^{-1})	Residues participating in intermolecular hydrogen bonds with 1BKV collagen			Residues involved in hydrophobic contacts with 1BKV collagen		
		Residues	Atoms*	Distance (nm)	Pi-sigma	Pi-alkyl	Alkyl
1BKV collagen	-205.30	Arg5	NH:O	3.14	Phe4, Phe20	Phe4, Phe19	Val12, Ile31, Val40, Ile41, Ala42
		Asp23	O:OH	1.76			

*The atoms on the left correspond to Aβ42 residues and atoms on the right correspond to 1BKV collagen.

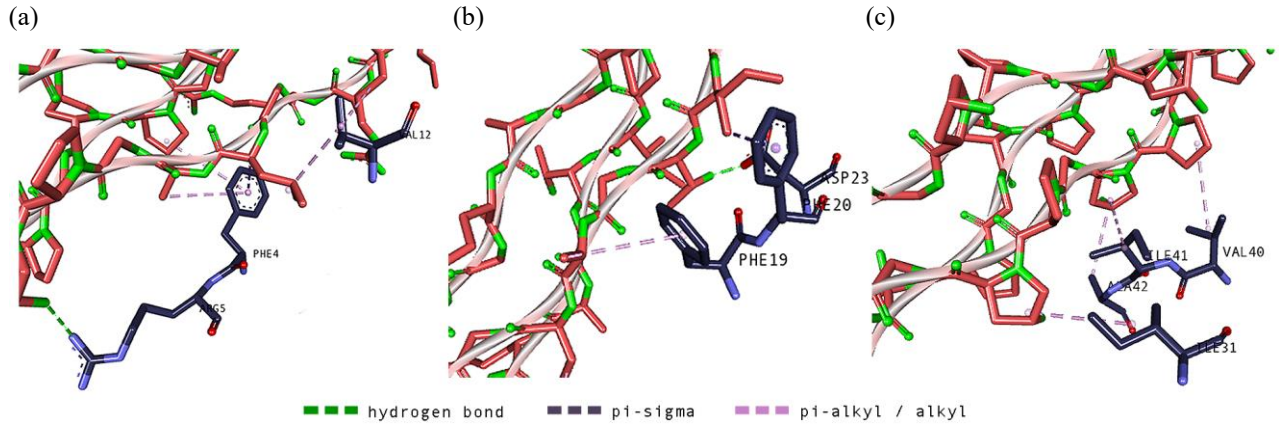

Figure 2. 3D binding interactions of Aβ42-1BKV collagen complex at different regions: (a) N-terminal, (b) CHC and turn and (c) SHR and C-terminal. The type of binding between the Aβ42 peptide and the 1BKV collagen is colour-coded as shown in the legend.

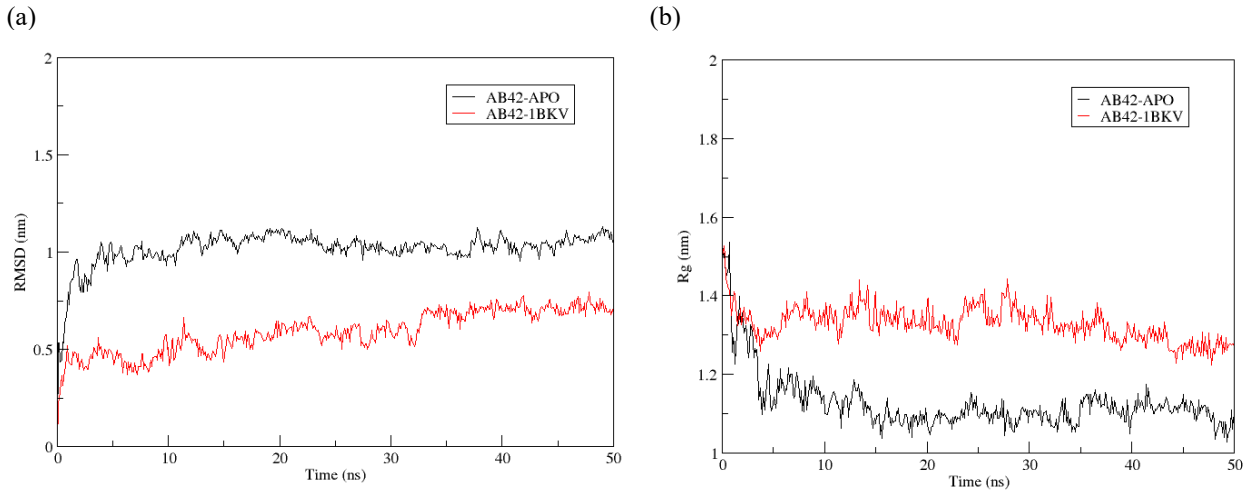

Figure 3. The root-mean-square deviation (RMSD) and radius-of-gyration (Rg) of Aβ$_{42}$-APO (black) and the Aβ$_{42}$-1BKV collagen complex (red) during simulations are shown in (a) and (b), respectively.

The global structural stability of the Aβ$_{42}$ peptide was assessed by calculating RMSD and Rg values over a trajectory of 50 ns in each system. The RMSD analysis serves as a measure for monitoring the degree of conformational changes of Aβ$_{42}$-APO and Aβ$_{42}$-1BKV that may occur during MD simulations. Figure 3(a) shows that the average RMSD value for the Aβ$_{42}$-1BKV collagen complex was lower than that of Aβ$_{42}$-APO, suggesting that collagen may contribute to the conformational changes of the Aβ$_{42}$ structure. For the AB$_{42}$-APO system, the RMSD remained within an average value of 1.02 nm, indicating that the Aβ$_{42}$ peptide did not change significantly from its native conformation. The Aβ$_{42}$-1BKV showed more fluctuation throughout the 50 ns in the Aβ$_{42}$ structure which indicated that the Aβ$_{42}$-1BKV collagen complex structure was quite unstable compared with AB$_{42}$-APO. The Aβ$_{42}$-1BKV showed an increase in RMSD during the last 20 ns of the simulation indicating significant changes in the conformation of AB$_{42}$ in the presence of collagen. The large variation in conformation may be one of the factors contributing to the destabilization of the native structure of the Aβ$_{42}$ peptide upon formation of a β-sheet structure.

The radius of gyration (Rg) is a measure of the compactness of any protein structure. In Figure 3(b), the average Rg values of the Aβ$_{42}$ peptide in the Aβ$_{42}$-APO and Aβ$_{42}$-1BKV collagen complex systems after 50 ns of simulation were found to be ~1.1 nm (which correlates with previous experimental results [32,33]) and ~1.3 nm, respectively, suggesting the role of 1BKV collagen in destabilizing the native structure of the Aβ$_{42}$ peptide. A larger fluctuation in the Rg value of the Aβ$_{42}$-1BKV collagen complex system implies higher perturbation, which increases the mobility of the Aβ$_{42}$ peptide.

The solvent accessible surface area (SASA) is an important property for determining protein conformations in water, and it gives a fair idea of the area that is exposed to solvent, accounting for interactions with hydrophobic and hydrophilic residues. An exposed surface area of hydrophobic residues is known to be crucial for the recognition and assembly of fibrils**.** It is also well known that β-sheets are stabilized by hydrophobic effects and helices are stabilized by the hydrophilicity of residues [34]. Generally, in terms of SASA, the stability of the Aβ$_{42}$ peptide is assessed by a decrease in area for hydrophobic residues and an increase in area for hydrophilic residues [35]. The SASA per residue was computed for both Aβ$_{42}$-APO and the Aβ$_{42}$-1BKV collagen complex. As seen in Figure 4, the SASA values of the CHC (residues 16-20) and C-terminal (residues 36-42) regions of the Aβ$_{42}$-1BKV collagen complex were higher compared to those of Aβ$_{42}$-APO. This result indicates that residues in this region had a higher propensity to self-assemble and aggregate [36]. It is clear that the hydrophobicity of central helix residues increased in the Aβ$_{42}$-1BKV collagen complex. This increase in hydrophobicity was directly related to the destabilization of the helix structure of the Aβ$_{42}$ peptide.

A feasible approach to halting the progression of Aβ$_{42}$ aggregation was to stabilize the helical native structure of the Aβ$_{42}$ peptide and avert Aβ$_{42}$ aggregation [37]. The secondary structure analysis was performed to analyse the effect of 1BKV collagen on the conformational landscape of the Aβ$_{42}$ peptide using the DSSP program [31]. As seen in Table 2 and Figure 5, the secondary structure component statistics indicated that Aβ$_{42}$-APO attained 32% coil, 0% β-content, 16% bend, 7% turn, and 45% helix conformations. On the other hand, the population percentage for coil, β-content, bend, turn, and helix

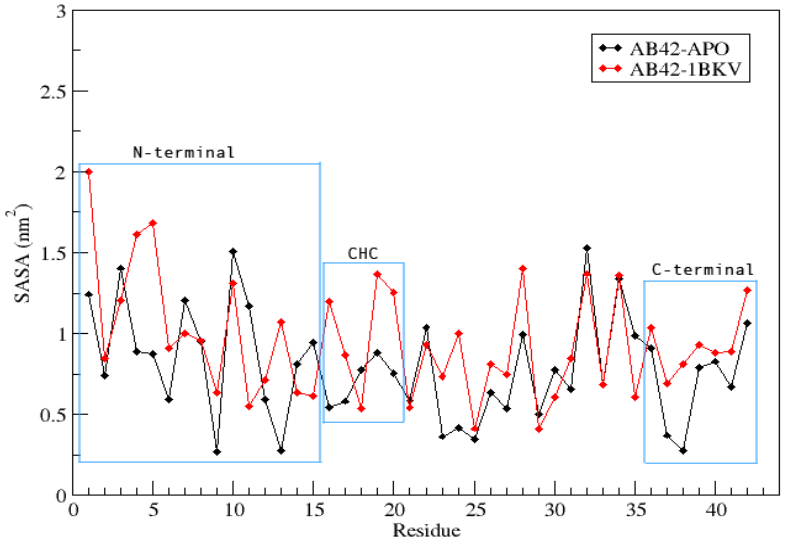

Figure 4. The solvent accessible surface areas (SASA) per residue of Aβ$_{42}$-APO (black) and the Aβ$_{42}$-1BKV collagen complex (red).

Table 2. The secondary structural component statistics for the Aβ$_{42}$-APO and Aβ$_{42}$-1BKV collagen complexes during MD simulations in water as explicit solvent.

Secondary Structure	**Aβ$_{42}$-APO** (%)	**Aβ$_{42}$-1BKV** (%)
Coil	32	32
β-content	0	3
Bend	16	14
Turn	7	18
Helix-content	45	33

Note: β-content is the sum of β-sheet and β-bridge.
Helix-content is the sum of α, 5 and 3-helix.

were found to be 32%, 3%, 14%, 18% and 33%, respectively for the Aβ$_{42}$-1BKV collagen complex. The DSSP analysis revealed an increase in the β-content (0% to 3%) which is a prerequisite for fibrillogenesis [3] along with a concomitant increase in turn (7% to 18%) and a decrease in the helical structure (45% to 33%) of the Aβ$_{42}$-1BKV complex compared to Aβ$_{42}$-APO, indicating that the 1BKV collagen destabilized the helical native structure of the Aβ$_{42}$ peptide.

To visualize the conformational changes in Aβ$_{42}$-APO and the Aβ$_{42}$-1BKV complex, snapshots were extracted at various time intervals (0, 10, 20, 30, 40, and 50 ns) from both systems (Figure 5). A visual inspection of the Aβ$_{42}$-APO trajectory revealed that after 5 ns, the C-terminus region was completely loose and formed a random-coil structure. This result agreed with a previous theoretical study which proved that Aβ rapidly transforms to a random coil conformation under solvation conditions [38]. Similar to Aβ$_{42}$-APO, the Aβ$_{42}$-1BKV collagen complex also formed a random-coil structure at the C-terminal with increasing β-content at the N-terminal. The random coil with β-sheet conformations of Aβ have been thought to assist the self-aggregation of Aβ oligomers [39].

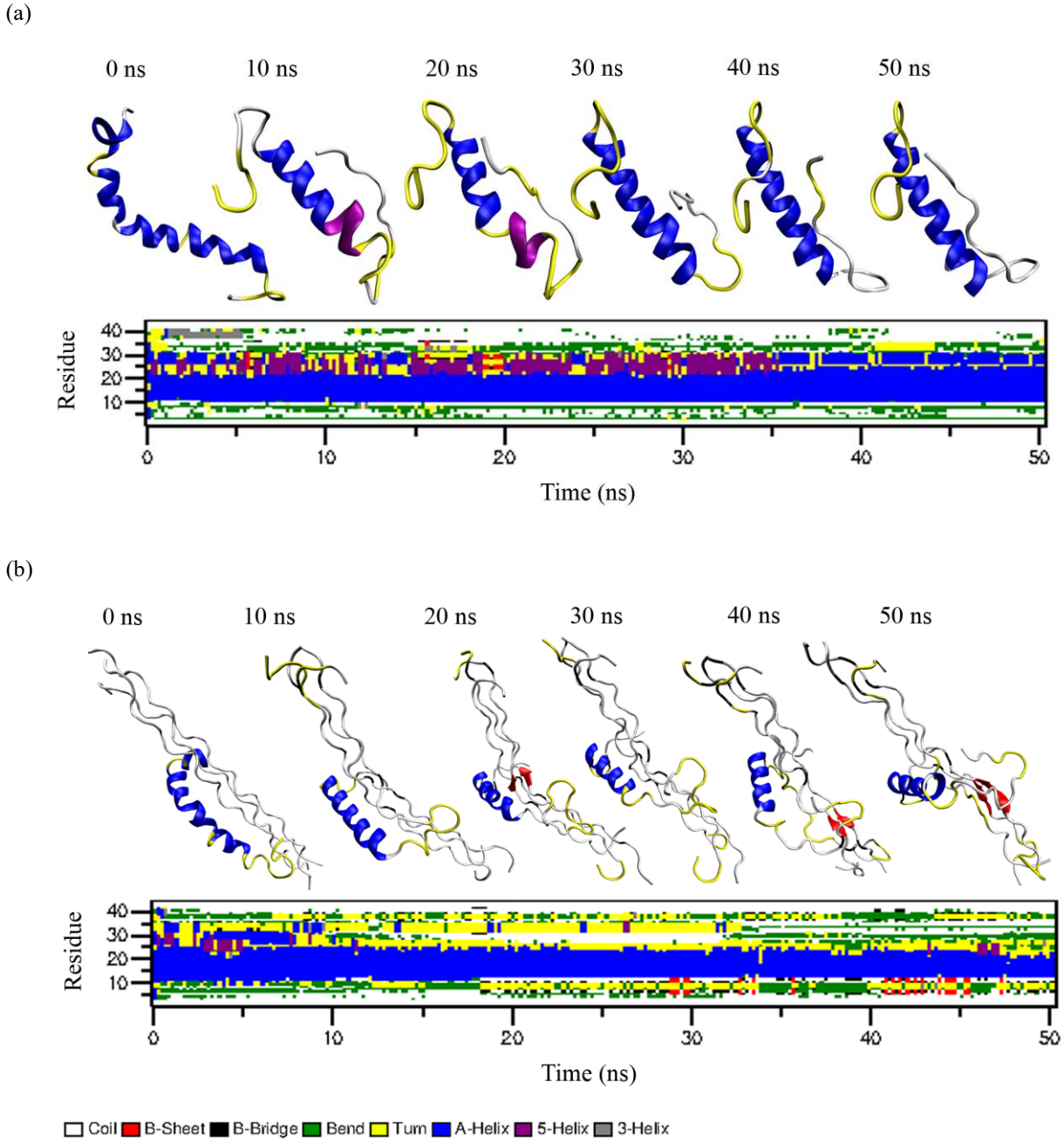

Figure 5. The snapshots and evolution of secondary structures for Aβ$_{42}$-APO (a) and the Aβ$_{42}$-1BKV complex (b) evaluated using DSSP in water. The Y-axis represents Aβ$_{42}$ residues and the X-axis represents simulation time in ns. The secondary structure of Aβ$_{42}$ is colour-coded as shown in the legend.

H-bonds are believed to play a major role in the formation of secondary structures and other higher-order aggregates by contributing immensely to structural integrity. The total number of hydrogen bonds were evaluated during the simulations for Aβ$_{42}$-APO and the Aβ$_{42}$-1BKV collagen complex (Figure 6(a)). The average number of hydrogen bonds were noted to be 25.283 and 21.962 for Aβ$_{42}$-APO and the Aβ$_{42}$-1BKV collagen complex, respectively. The decreased number of hydrogen bonds in Aβ$_{42}$-1BKV was associated with a decrease in the helical conformation of the Aβ$_{42}$ peptide in Aβ$_{42}$-1BKV. The number of hydrogen bonds between Aβ$_{42}$ and 1BKV collagen were evaluated during simulations, with an average of 9.780 hydrogen bonds observed (Figure 6(b)). The hydrogen bond analysis confirmed the strong binding of 1BKV collagen with Aβ$_{42}$.

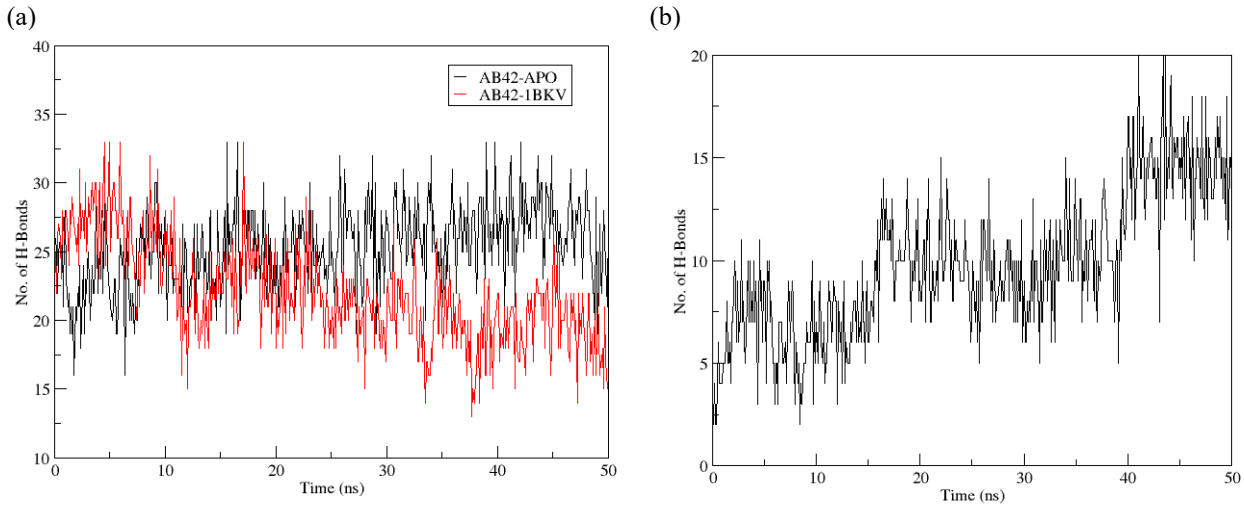

Figure 6. The total number of hydrogen bonds summed over each frame of the trajectory during simulations for the $A\beta_{42}$-APO (black) and $A\beta_{42}$-1BKV collagen complexes (red) in (a). The number of hydrogen bonds between $A\beta_{42}$ and 1BKV collagen during simulations is shown in (b).

CONCLUSION

In the present study, the binding interactions of type III collagen with a $A\beta_{42}$ monomer and the conformational dynamics of the $A\beta_{42}$ monomer were investigated through molecular docking and MD simulations. The molecular docking analysis highlighted that 1BKV collagen formed hydrogen bonds with Arg5 and Asp23 and hydrophobic contacts with residues of N-terminal (Phe4, Val12), CHC (Phe19, Phe20), SHR (Ile31) and C-terminal (Val40, Ile41, Ala42) regions of the $A\beta_{42}$ monomer. MD simulations revealed that type III collagen reduced the helical content (44% to 33%) and promoted the aggregation-prone β-sheet conformation (0% to 3%) in the $A\beta_{42}$ peptide structure.

ACKNOWLEDGEMENT

The authors gratefully acknowledge financial support from the Graduate Research Fellowship (GRF) and GP-IPM Vote Number: 9628900 grant from Universiti Putra Malaysia (UPM) to support this work.

REFERENCES

1. Liu, P. P., Xie, Y., Meng, X. Y. and Kang, J. S. (2019) History and progress of hypotheses and clinical trials for Alzheimer's disease. *Signal Transduction and Targeted Therapy*, **29(2019).**

2. Hardy, J. A. and Higgins, G. A. (1992) Alzheimer's Disease: the Amyloid Cascade Hypothesis. *Science*, **256(5054)**, 184−185.

3. Rosenman, D. J., Connors, C. R., Chen, W., Wang, C. Y. and Garcia, A. E. (2013) A beta Monomers Transiently Sample Oligomer and Fibril-Like Configurations: Ensemble Characterization Using a Combined MD/NMR Approach. *J. Mol. Biol.*, **425(18)**, 3338−3359.

4. Ma, J., Ma, C., Li, J., Sun, Y., Ye, F., Liu, K. and Z, H. (2020) Extracellular matrix proteins involved in Alzheimer's disease. *Chemistry, A European Journal*, **26(53)**, 12101−12110.

5. Hubert, T., Grimal, S., Carroll, A. and Fichard-Carroll, A. (2009) Collagens in the developing and diseased nervous system. *Cellular and Molecular Life Sciences*, **66(7)**, 1223−1238.

6. Barros, C. S., Franco, S. J. and Muller, U. (2011) Extracellular Matrix: Functions in the Nervous System. *Cold Spring Harbor Perspectives in Biology*, **3(1)**, a5108.

7. Song, I. and Dityatev, A. (2018) Crosstalk between glia, extracellular matrix and neurons. *Brain Res Bull*, **136(1)**, 101−108.

8. Fawcett, J. W., Oohashi, T. and Pizzorusso (2019) The roles of perineuronal nets and the perinodal extracellular matrix in neuronal function. *Nature Reviews Neuroscience*, **20**, 451–465.

9. Hillen, A. E. J., Burbach, J. P. H. and Hol, E. M. (2018) Cell adhesion and matricellular support by astrocytes of the tripartite synapse. *Prog. Neurobiol.*, **165-167**, 66−68.

10. Cheng, J. S., Dubal, D. B., Kim, D. H., Legleiter, J., Cheng, I. H., Tesseur, I., Wyss-Coray, T., Bonaldo, P. and Mucke, L. (2009) Collagen VI protects neurons against Abeta toxicity, *Nature Neuroscience*, **12(2)**, 119−121.

11. Söderberg, L., Dahlqvist, C., Kakuyama, H., Thyberg, J., Ito, A., Winblad, B., Näslund, J. and Tjernberg, L. O. (2005) Collagenous Alzheimer amyloid plaque component assembles amyloid fibrils into protease resistant aggregates. *The FEBS Journal*, **272(9)**, 2331−2236.

12. Kramer, R. Z., Bella, J., Mayville, P., Brodsky, B. and Berman, H. M. (1999) Sequence dependent conformational variations of collagen triple-helical structure. *Nature Structural Biology*, **6(5)**, 454−457.

13. Tomaselli, S., Esposito, V., Vangone, P., Van Nuland, N. A. J., Bonvin, A. M. J. J., Guerrini, R., Tancredi, T., Temussi, P. A. and Picone, D. (2006) The alpha-to-beta conformational transition of Alzheimer's Abeta-(1-42) peptide in aqueous media is reversible: a step by step conformational analysis suggests the location of beta conformation seeding, *ChemBioChem*, **7(2)**, 257–267.

14. Yan, Y., Tao, H., He, J. and Huang, S. (2020) The HDOCK server for integrated protein–protein docking, *Nature Protocols*, **15(5)**, 1829–1852.

15. DS BIOVIA - Dassault Systèmes BIOVIA: San Diego, CA, USA, 2019.

16. Abraham, M. J., Murtola, T., Schulz, R., Pall, S., Smith, J. C., Hess, B. and Lindahl, E. (2015) GROMACS: High performance molecular simulations through multi-level parallelism from laptops to supercomputers, *SoftwareX*, **1–2**, 19−25.

17. Daura, X., Mark, A. E. and van Gunsteren, W. F. (1998) Parameterization of aliphatic CHn united atoms of GROMOS96 force field. *Journal of Computational Chemistry*, **19(5)**, 535–547.

18. Shuaib, S. & Goyal, B. (2018) Scrutiny of the mechanism of small molecule inhibitor preventing conformational transition of amyloid-β_{42} monomer: insights from molecular dynamics simulations. *Journal of Biomolecular Structure and Dynamics*, **36(3)**, 663−678.

19. Yang, C., Zhu, X., Li, J. and Shi, R. (2010) Exploration of the mechanism for LPFFD inhibiting the formation of β-sheet conformation of Aβ(1–42) in water. *J. Mol. Model*, **16**, 813–821.

20. Viet, M. H., Ngo, S. T., Lam, N. S. and Li, M. S. (2011) Inhibition of Aggregation of Amyloid Peptides by Beta-Sheet Breaker Peptides and Their Binding Affinity. *The Journal of Physical Chemistry B*, **115(22)**, 7433−7446.

21. Viet, M. H. and Li, M. S. (2012) Amyloid peptide Aβ40 inhibits aggregation of Aβ42: evidence from molecular dynamics simulations. *J. Chem. Phys.*, **136(24)**, 245105.

22. Liu, F., Du, W., Sun, Y. and Dong, X. (2014) Atomistic characterization of binding modes and affinity of peptide inhibitors to amyloid-β protein. *Frontiers of Chemical Science and Engineering*, **8**, 433–444.

23. Xie, L., Luo, Y., Lin, D., Xi, W., Yang, X. and Wei, G. (2014) The molecular mechanism of fullerene-inhibited aggregation of Alzheimer's β-amyloid peptide fragment. *Nanoscale*, **6(16)**, 9752−9762.

24. Saini, R. K., Shuaib, S., Goyal, D. and Goyal, B. (2018) Insights into the inhibitory mechanism of a resveratrol and clioquinol hybrid against $A\beta_{42}$ aggregation and protofibril destabilization: A molecular dynamics simulation study. *Journal of Biomolecular Structure and Dynamics*, **37(12)**, 3183−3197.

25. Berendsen, H. J. C., Postma, J. P. M., van Gunsteren and Hermans, J. (1981) Interaction Models for Water in Relation to Protein Hydration. *Intermolecular Forces*, **11(1)**, 331−342.

26. Darden, T., York, D. and Pedersen, L. (1993) Particle mesh Ewald: An $N\cdot\log(N)$ method for Ewald sums in large systems. *The Journal of Chemical Physics*, **98(12)**, 10089−10092.

27. Hess, B., Bekker, H., Berendsen, H. J. C. and Fraaije, J. G. E. M. (1998) LINCS: A linear constraint solver for molecular simulations. *Journal of Computational Chemistry*, **18(12)**, 1436−1472.

28. Cuendet, M. A. and van Gunsteren, W. F. (2007) On the calculation of velocity-dependent properties in molecular dynamics simulations using the leapfrog integration algorithm. *Journal of Chemical Physics*, **127(18)**, 184102.

29. Bussi, G., Donadio, D. and Parrinello, M. (2007) Canonical sampling through velocity rescaling. *Journal of Chemical Physics*, **126(1)**, 014101.

30. Parrinello, M. and Rahman, A. (1981) Polymorphic transitions in single crystals: A new molecular dynamics method. *Journal of Applied Physics*, **52(12)**, 7182−7190.

31. Kabsch, W. and Sander, C. (1983) Dictionary of protein secondary structure: pattern recognition of hydrogen-bonded and geometrical features. *Biopolymers*, **22(12)**, 2577−637.

32. Gerben, S. R., Lemkul, J. A., Brown, A. M. and Bevan, D. R. (2014) Comparing atomistic molecular mechanics force fields for a difficult target: a case study on the Alzheimer's amyloid β-peptide. *Journal of Biomolecular Structure and Dynamics*, **32(11)**, 1817–1832.

33. Nag, S., Sarkar, B., Bandyopadhyay, A., Sahoo, B., Sreenivasan, V. K. A., Kombrabail, M. and Maiti, S. (2011) Nature of the amyloid-β monomer and the monomer–oligomer equilibrium. *Journal of Biological Chemistry*, **286(16)**, 13827–13833.

34. Berhanu, W. M. and Masunov, E. (2011) Molecular dynamic simulation of wild type and mutants of the polymorphic amyloid NNQNTF segments of elk prion: Structural stability and thermodynamic of association. *Biopolymers*, **95(9)**, 573–590.

35. Berhanu, W. M. and Hansmann, U. H. E. (2012) Side-chain hydrophobicity and the stability of Ab16-22 aggregates. *Protein Science*, **21(12)**, 1837–1848.

36. Mehrazma, B. and Rauk, A. (2019) Exploring Amyloid-β Dimer Structure Using Molecular Dynamics Simulations. *The Journal of Physical Chemistry*, **123(22)**, 4658−4670.

37. Thu, T. T. M., Co, N. T., Tu, L. A. and Li, M. S. (2019) Aggregation rate of amyloid beta peptide is controlled by beta-content in monomeric state. *Journal of Chemical Physics*, **150(22)**, 225101.

38. Lee, C. and Ham, S. (2011) Characterizing Amyloid-Beta Protein Misfolding from Molecular Dynamics Simulations with Explicit Water. *Journal of Computational Chemistry*, **32(2)**, 349–355.

39. Yang, C., Li, J., Li, Y. and Zhu, X. (2009) The effect of solvents on the conformations of Amyloid β-peptide (1–42) studied by molecular dynamics simulation. *Journal of Molecular Structure*, **895(2009)**, 1−8.